

# Finite element analysis of nanoindentation responses of TiB<sub>2</sub> coatings with a Ti interlayer on high speed steel

N. Panich<sup>1</sup>, P. Wangyao<sup>1</sup>, J. Zrník<sup>2,3\*</sup>, S. Surinphong<sup>4</sup>, Y. K. Tan<sup>5</sup>, Y. Sun<sup>6</sup>

<sup>1</sup> *Metallurgy and Materials Science Research Institute, Chulalongkorn University, Bangkok, Thailand*

<sup>2</sup> *Comtes FHT, Lobežská E-981, 326 00 Pilsen, Czech Republic*

<sup>3</sup> *Materials Science Department, Faculty of Metallurgy, Technical University, Košice, Slovak Republic*

<sup>4</sup> *NanoShield Co., Ltd., Samutprakarn, Thailand*

<sup>5</sup> *School of Materials Science & Engineering, Nanyang Technological University, Singapore*

<sup>6</sup> *School of Engineering & Technology, De Montfort University, Leicester LE1 9BH, United Kingdom*

Received 23 July 2007, received in revised form 16 October 2007, accepted 4 December 2007

## Abstract

In the present work, the development of finite element (FE) models to simulate the nanoindentation processes in various TiB<sub>2</sub>-based nanostructured coatings was investigated. The developed nanoindentation FE models were able to simulate the indentation loading-unloading curves of the coating/substrate system. The model could also be used to extract the intrinsic values of mechanical properties, e.g. hardness and yield strength. In addition, the models were used to analyse the plastic deformation behaviour of coating-substrate systems during indentation process and investigate the effect of penetration depth on nanoindentation.

**Key words:** TiB<sub>2</sub>-based nanostructured coating, nanoindentation, finite element analysis, hardness, modulus, plastic deformation

## 1. Introduction

Increasing applications have been found for thin, hard, wear resistant (ceramic) coatings in metal cutting and metal forming tools. The invention of low temperature (below 500 °C) physical vapour deposition (PVD) processes such as magnetron sputtering has made possible the deposition of various hard and wear resistant coatings onto commonly used tool steels. When applied properly, protective coatings on cutting tools and other tribological components can extend component lifetime. It is usually desirable to have coating with high hardness and low internal stress. Among the many materials of interest, titanium diboride (TiB<sub>2</sub>) has notably been chosen. TiB<sub>2</sub> possesses many interesting physical, mechanical and chemical properties, such as high hardness, high melting point, good chemical stability and good thermal and electrical conductivity. There have been increasing interests in fabrication of this material in thin film and coating forms for many potential applications.

Since many technologies have moved to ever small-

er scale, characterization of the intrinsic mechanical properties of materials and thin films has become more difficult and complicated. Among the techniques to measure the mechanical properties of nanostructured thin films, nanoindentation techniques have been widely used to measure thin film mechanical properties, for instance hardness, elastic modulus, scratch resistance, creep, etc. Other reasons for the popularity of the nanoindentation method are that the mechanical properties can be measured without removing the film from its substrate as is done in other types of testing and that it provides the ability to probe a surface at numerous points, in both lateral and depth dimensions. In order to obtain the intrinsic properties of thin film materials, it is essential that the effect of the underlying substrate is eliminated during the test and/or through proper modelling and simulation.

Different numerical methods have been developed and can be used in indentation problems. Bhattachaya and Nix [1] used the finite element (FE) technique with a two-dimensional (2-D) model to solve the in-

\*Corresponding author: tel.: 00420 377 327427; fax: 00420 377 422224; e-mail address: [jzrnik@comtesfht.cz](mailto:jzrnik@comtesfht.cz)

dentation problem with an axisymmetric conical indenter. This cone shape is constrained to have the same volume as a pyramid-shaped indenter for a given depth. Their FE hardness results compared well with experimental data. They also presented an elastoplastic analysis of axisymmetric conical indenter and showed that the shape of the plastic zone strongly relies on the indentation angle, Young's modulus and yield stress [2]. Sun et al. [3] developed an axisymmetric FE model to simulate the indentation of coating-substrate systems using a conical indenter. The axisymmetric indenter is constrained to have the same projected area of the Berkovich indenter, as a function of the indentation depth. Chollacoop et al. [4] analysed the approach to interpret the instrumented sharp indentation with usual sharp indenters with different tip angles. The model was developed to improve the accuracy and sensitivity of the algorithms used to extract the mechanical properties. Three-dimensional (3-D) FE models have been developed to investigate the indentation response in coated systems and bulk materials by Licinchi et al. [5], Wang and Bangret [6], and Knapp and Follstaedt [7], whilst Muliana used an artificial neural network (ANN) technique for nanoindentation processes simulation [8]. The complex deformation field is demonstrated by the 3-D model as well as the load and displacement curves. It was found that the load and displacement curves extracted from the 2-D model compare well to results from the 3-D model, showing that the 2-D model is computationally affordable [5]. Kennedy and Ling [9] used the FE method to analyse the indentation problem of a thin elastic-plastic coating deposited on different substrates. They showed that the indenter size, the contact pressure, the coating thickness, and the coating and substrate properties affect the yielding event. Komvopoulos [10] used elastic-plastic FE analysis to calculate the stress distribution of an indented ceramic coating on a metallic substrate. It was shown that the coating thickness and the mechanical properties of the coating and the substrate significantly affect the contact pressure profile on the contact surface. Also, it was found that yielding in the layered medium always initiates at the coating-substrate interface below the centre of contact and the plastic zone does not grow toward the surface of the indented layered medium but is restricted to the boundary of the hard coating and the substrate. Similar FE analysis of a rigid indenter on an elastoplastic two-layered system has been conducted by other investigators [11, 12]. The Hertz theory and FEM have been combined by Djabella and Arnell [13] to analyse elastic stresses in single, double and multilayer systems.

In the present paper, attempts have been made to develop the nanoindentation models which are able to simulate the indentation loading-unloading curves of the coating/substrate system. The model of the single-

-layer ceramic coating with a Ti interlayer has been developed in this work by simulating the real coating/substrate condition such as coating thickness. In order to enhance the accuracy of the model, the indenter tip radius was modelled using the same geometry as the real tip radius in nanoindentation experiment. The models have the ability to simulate the loading-unloading curves, to study the influence of film structure and properties on indentation response, to simulate the development of plastic deformation during indentation.

## 2. Finite element modelling

Since coatings have been designed by having an interlayer such as Ti, single layer TiB<sub>2</sub> coating on high-speed steel substrate with a Ti interlayer was developed instead of mere single-layer model. The indentation process under consideration involves a coating perfectly adherent to an interlayer and a substrate indented by a rigid indenter under the condition of frictionless contact. The indenter has a half-angle of 70.3°, and thus has the same projected area-depth function as the standard Berkovich indenter. The use of a conical indenter simplifies the analysis to a two dimension (2-D) axisymmetric problem. Accordingly, the indentation process can be modelled with the finite element mesh shown in Fig. 1. A total of 1892 four-node axisymmetric reduced integration elements (CAX4R element type [14]) were used to model the semi-infinite layered medium. A very fine mesh was used in the coating and the substrate adjacent to the contact zone. The mesh was continuously coarsened further away from the contact area. Three element sets, one corresponding to the coating, one corresponding to the Ti-interlayer and the other to the substrate, were used to define separately the elastic and plastic properties of the coating, interlayer and the substrate materials (Fig. 1).

In order to detect the contact between the coating surface and the rigid indenter, the contact constraint was defined by choosing the indenter as the master surface and the coating surface as the slave surface, where only the master surface can penetrate into the slave surface. The contact or separation between the master surface and slave surface nodal points was automatically detected and monitored in the programme.

The boundary conditions of the present model are also illustrated in Fig. 1. Roller boundary conditions were applied to the centreline and bottom surface nodes, whilst the outer right-hand side nodes were assumed traction-free. The validity of the described finite element model and programme has been tested by comparing the finite element results for the elastic contact between a half-space and a rigid sphere, with

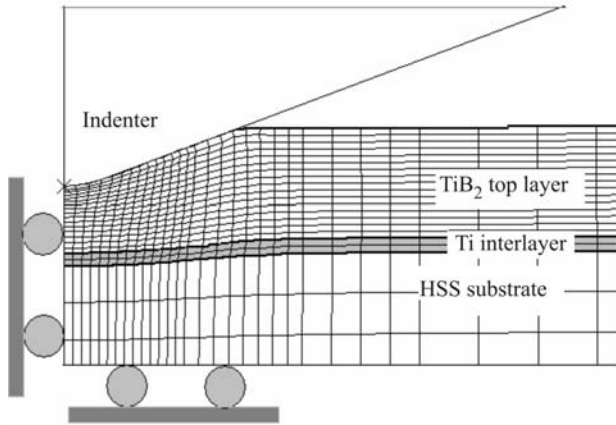


Fig. 1. The finite element mesh and boundary conditions with the details of the mesh in the region near the tip of the indenter during the loading stage.

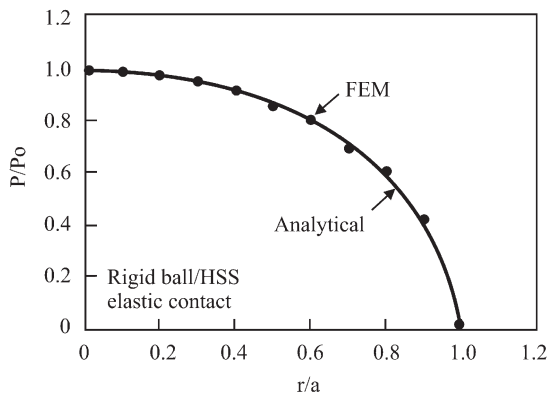


Fig. 2. Pressure distribution in the contact zone obtained by the FE and the analytical solutions of elastic contact between the HSS half-space and a rigid sphere ( $a$  – half-contact width;  $r$  – distance from contact centre) [3].

Table 1. Mechanical properties of TiB<sub>2</sub> used in the FE model

No.	Young's modulus $E$ (GPa)	Yield strength $Y$ (GPa)	Poisson's ratio
1	250	10	0.25
2	250	12	0.25
3	260	11	0.25
4	260	12	0.25
5	260	13	0.25
6	270	12	0.25
7	270	13	0.25
8	300	10	0.25

the results of the analytical Hertz solution. Figure 2 indicates the normalized pressure distribution along the radius of the contact zone. It can be seen that very good agreement has been achieved between the FE

Table 2. Mechanical properties of Ti, TiB<sub>2</sub> and HSS used in the FE model

Material	Young's modulus $E$ (GPa)	Yield strength $Y$ (GPa)	Poisson's ratio
Ti	200	0.5	0.30
TiB <sub>2</sub>	250–300	10–13	0.25
HSS	225	4	0.30

and the analytical solutions [3]. The developed model has the ability to simulate the load-unload stages of the indentation process of any single-layer coating system, to study the plastic deformation behaviour in the coating on substrate and to extract mechanical properties from experimental indentation tests.

For the purpose of using the developed model to extract the intrinsic mechanical properties of the coating system, several combinations of modulus ( $E_{TiB_2}$ ) and yield strength ( $Y_{TiB_2}$ ) of TiB<sub>2</sub> coating were used in the computation, as listed in Table 1, whilst the properties of Ti and HSS remained constant (Table 2). The hard coating and interlayer were perfectly adhered to the substrate and were indented by a rigid conical indenter. The set of  $E_{TiB_2}$  and  $Y_{TiB_2}$  that yields the best fit between the simulation load and unload curves and those of experiments is regarded as being the intrinsic properties of the TiB<sub>2</sub> coating.

For the experimental results, the Ti/TiB<sub>2</sub> coating was deposited onto the HSS substrate experimentally, with a thickness of 0.15  $\mu\text{m}$  and 1.25  $\mu\text{m}$  for Ti and TiB<sub>2</sub>, respectively, as illustrated in Fig. 3. Nanoindentation test was then performed with a Berkovich diamond indenter, to a depth of 50 nm.

In the calculation, the elastic deformation occurs in the beginning of the process. The von Mises' yield criterion is applied in the occurrence of the plastic deformation. The von Mises' stress equation is given by the expression

$$\sigma_{\text{Mises}} = \sqrt{\frac{(\sigma_1 - \sigma_2)^2 + (\sigma_2 - \sigma_3)^2 + (\sigma_3 - \sigma_1)^2}{2}}, \quad (1)$$

where  $\sigma_1$ ,  $\sigma_2$  and  $\sigma_3$  are the three principle stresses. When the  $\sigma_{\text{Mises}}$  reaches the yield strength ( $Y$ ), the specimen starts to deform plastically. There is no strain-hardening behaviour of the specimen considered in the model.

### 3. Simulation results

#### 3.1. The load-displacement curves and material sink-in

The typical loading and unloading curve of the

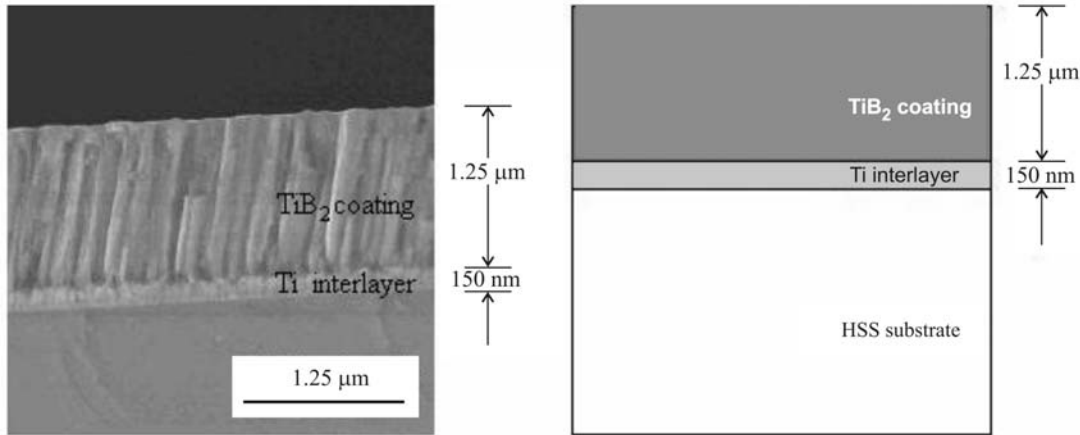


Fig. 3. The dimension of the Ti/TiB<sub>2</sub> coating, which follows the real coating dimension, used in this study.

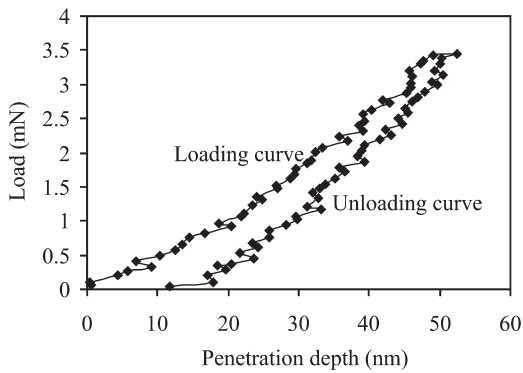


Fig. 4. Experimental loading and unloading curve of Ti/TiB<sub>2</sub> coating (sample 1 in Ref. [15]).

experimental nanoindentation test (sample 1 in Ref. [15]) was plotted, as shown in Fig. 4. This experimental load-displacement curve was used to compare with the simulation results to find out the best fit between FE and experimental results. Since the best fit was found, the important coating properties could be predicted by the FE model such as the yield stress ( $Y$ ) and elastic modulus ( $E$ ).

Load-displacement curves calculated by the FE model with different coating properties were plotted and compared with the experimental curve (Fig. 5a–h). The properties of the HSS substrate and Ti interlayer used in the models were fixed as shown in Table 2, whilst the properties of TiB<sub>2</sub> coating were varied (Table 1). Figure 5e shows the best fit of the FE curve to the experimental curve. Hence, it can be assumed that the mechanical properties of this TiB<sub>2</sub> coating are: Young's modulus  $E = 260$  GPa and yield strength  $Y = 13$  GPa. From this result, it is clear that with the FE technique, the properties of the coating could be derived, in particular the yield strength, which could not be extracted from experimental nanoindentation.

In order to extract the intrinsic mechanical properties such as hardness of TiB<sub>2</sub> coating by using the FE model, the model was inputted with the above mechanical properties i.e.  $E = 260$  GPa and  $Y = 13$  GPa and then the nanoindentation processes were simulated. Figure 6 shows the indentation profiles simulated for the HSS substrate alone, the coating material alone and the coating-substrate system at the same indentation depth of 500 nm. It can be seen that indentation of the substrate half-space alone and the coating half-space results in material sink-in as expected from the material properties of the hard materials [16]. The coating-substrate system experiences material sink-in, which is greater than the HSS substrate half-space.

To further demonstrate the phenomenon of material sink-in in the coating-substrate system, Fig. 7 compares the sink-in depth (i.e. the depth of the sink-in material with reference to the original surface of the coating) of the coating/substrate system with those of the corresponding coating half-space.

From Fig. 7 it can be seen that at indentation depth below  $0.2 \mu\text{m}$ , there is no difference in sink-in behaviour between the coating half-space and the coating-substrate system, indicating insignificant substrate effect. The sink-in effect in different penetration depth is further illustrated in Fig. 8 as obtained by the FE model. It can be seen that the sink-in depth increases as penetration depth increases.

From such indentation profiles, the true contact area could be derived by measuring the area where the indenter tip made contact with the coating (arrow in Fig. 8). This is regarded as the true contact area. The hardness calculated from the true area at 50 nm depth with the calculated maximum load of 2.6 mN is 24.48 GPa, which is in very good agreement with the experiment (sample 1 in Table 1 of [15]). Further investigation was conducted to calculate the true hardness of TiB<sub>2</sub> coating at different penetration depths, i.e. 100 nm, 200 nm, 300 nm, 400 nm and 500 nm. Table 3 summarizes the calculated true hardness

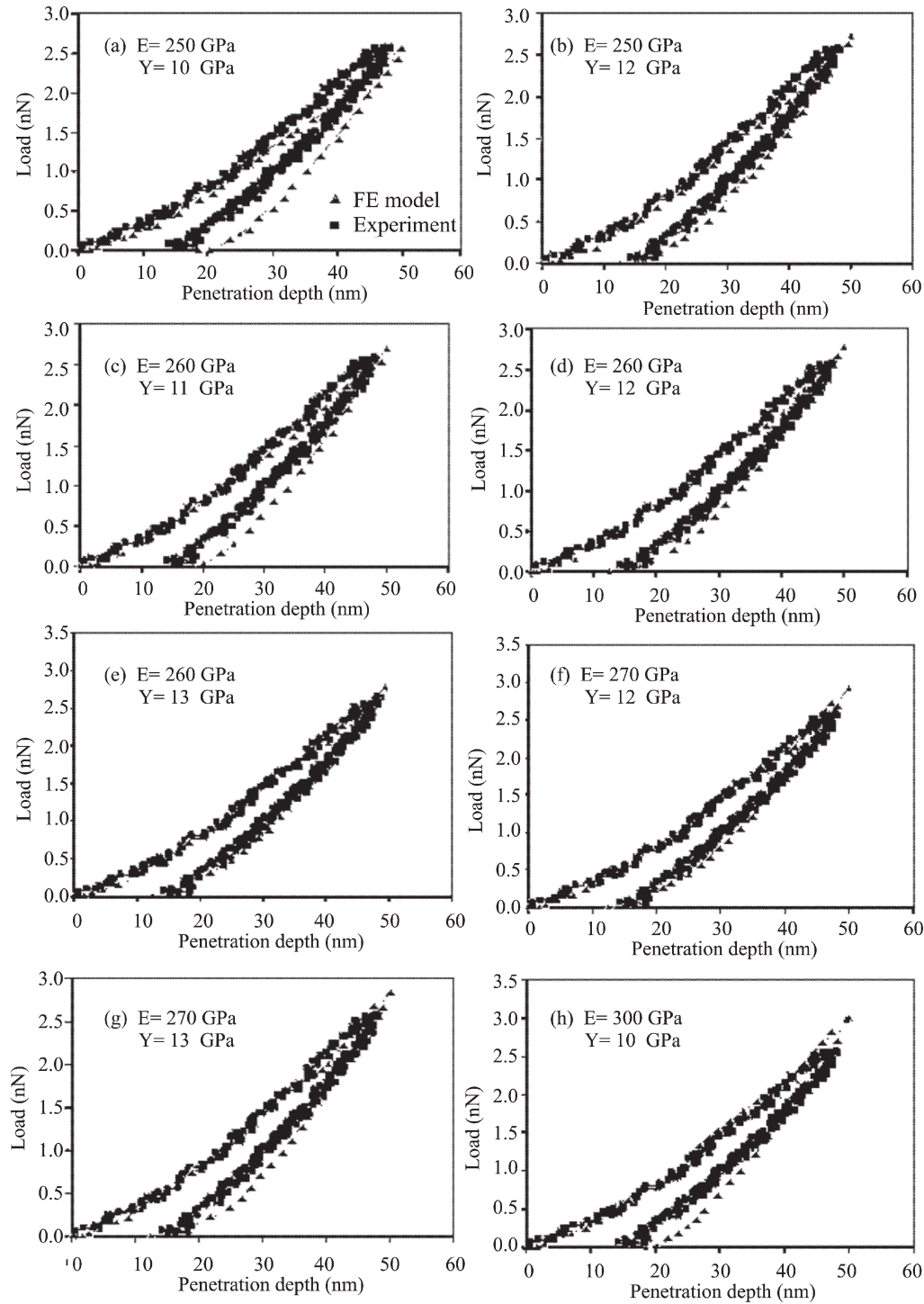


Fig. 5. Comparison of load-displacement curves between experiments and FE results to find the best fit of both curves.

of  $\text{TiB}_2$  coating at different depth by FE modelling.

Table 3 shows that the calculated hardness decreases with the increase in the penetration depth due to the substrate effect, which will be discussed later. The results of FE calculation and experimental measurements are compared in Fig. 9. Good agreement is evident from the figure.

Figure 10 shows the propagation of the plastic deformation zone in the  $\text{TiB}_2$  coating (with Ti inter-layer) and the HSS substrate during the nanoindentation process. At small indentation depths, plastic deformation occurs in the coating only, which propagates both vertically and laterally (Fig. 10a,b). At larger depths, the plastic zone in the coating reaches

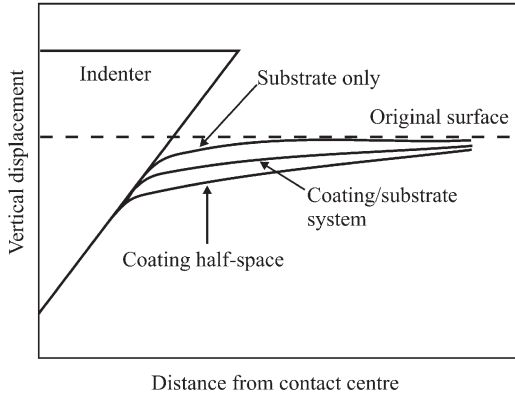


Fig. 6. Surface profiles of the indented coating/substrate system ( $\text{TiB}_2$  coating) and the corresponding substrate and coating half-space, showing sink-in in the coating/substrate system.

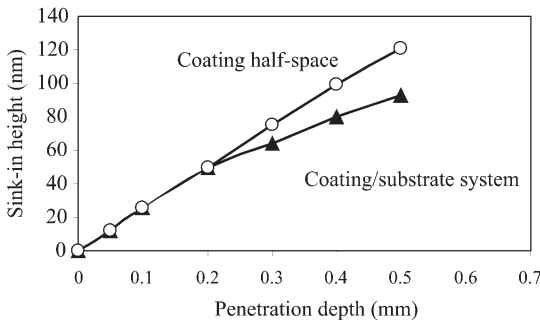


Fig. 7. Comparison of sink-in depth in the coating/substrate system and in the corresponding coating half-space, showing enhanced sink-in in the coating/substrate system after certain critical penetration depth.

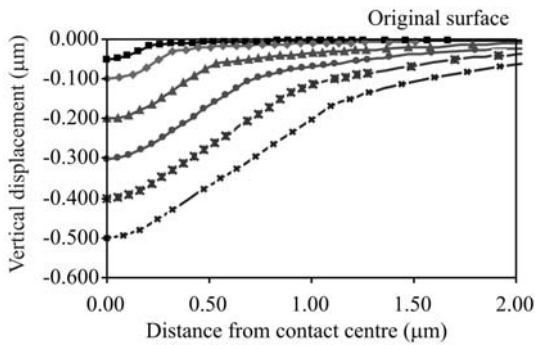


Fig. 8. The sink-in effect in different penetration depth in the interval 50–500 nm.

the coating/substrate interface, and then is constrained vertically, such that the zone only propagates along the lateral direction (Fig. 10c,d). Further increase in depth results in the further lat-

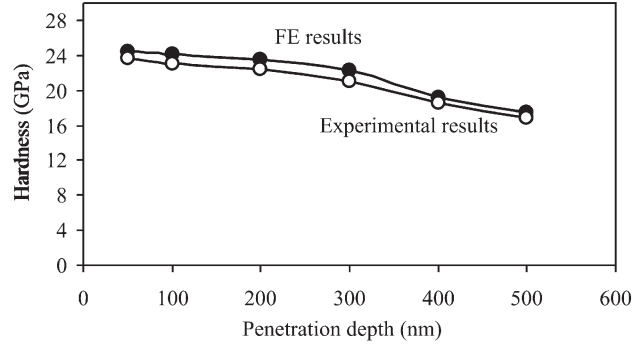


Fig. 9. Comparison between FE calculation and experimental results at different penetration depth.

Table 3. Calculated true hardness of  $\text{TiB}_2$  coating at different depth

Penetration depth (nm)	Calculated hardness (GPa)
50	24.48
100	24.16
200	23.48
300	22.20
400	19.15
500	17.50

eral propagation of the plastic zone in the coating, until a certain critical depth, at which plastic deformation in the substrate at the interface is initiated and then propagated (Fig. 10e). The plastic deformation occurred in the substrate will affect the measurement of the coating properties. The propagation of the plastic deformation zone in the Ti interlayer could not be shown in Fig. 10 because the Ti interlayer can be deformed easily due to its low yield strength. Once the indentation penetrated into the coating (at 50 nm), the plastic deformation zone in the Ti interlayer started immediately. This means that the plastic deformation zone in the Ti interlayer only propagates along the lateral direction.

Figure 10a–d shows that the HSS substrate is free from plastic deformation (yield strength of the HSS substrate is 4 GPa). However, a plastic zone started to form in the substrate when the indentation depth reached 365 nm (arrow in Fig. 10e). Therefore, it is necessary to avoid indenting above this depth in order to prevent the substrate from undergoing plastic deformation.

However, this result of critical indentation depth of 365 nm was over-calculated due to the influence of the soft Ti interlayer, which helps to accommodate the stress before it goes through the substrate [17]. This also proves the benefit of the thin interlayer to

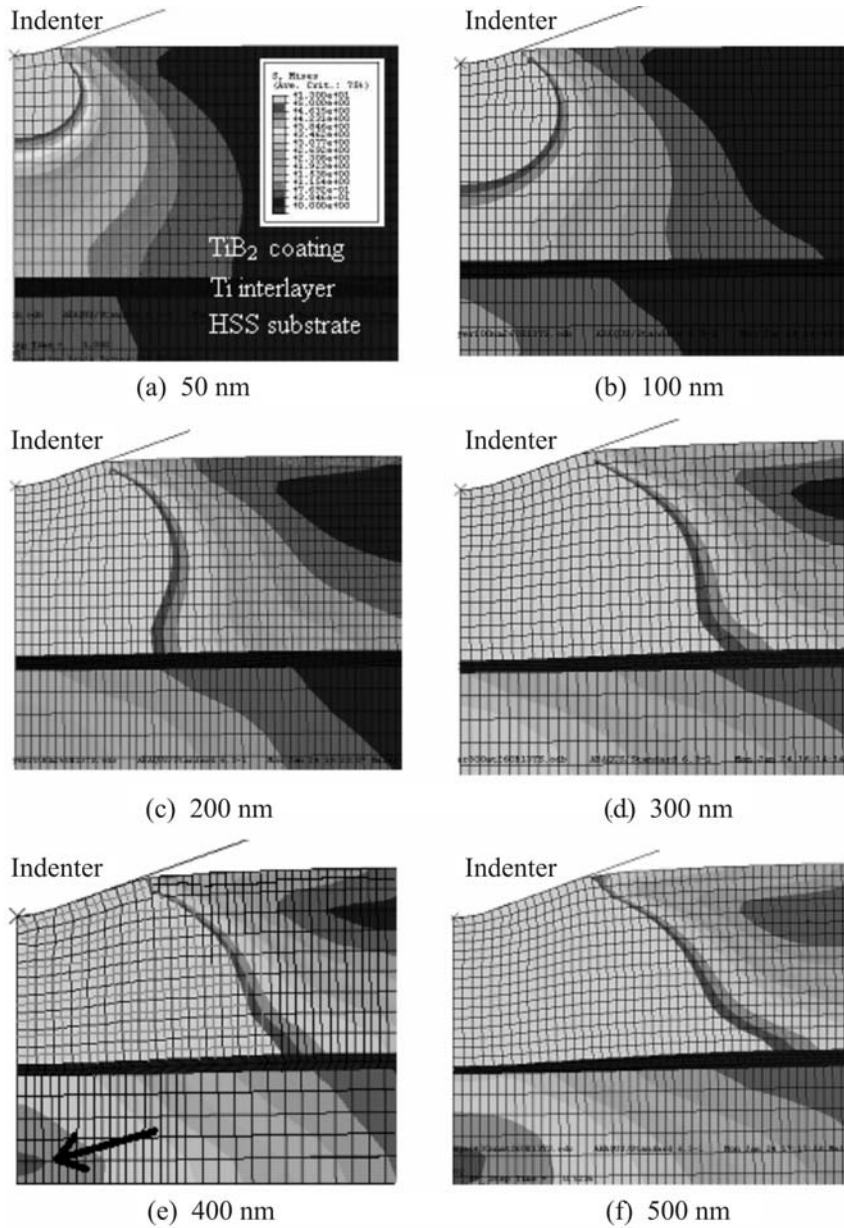


Fig. 10. Stress distribution in the TiB<sub>2</sub> coating with Ti interlayer on HSS substrate at different indentation depth: (a) 50 nm, (b) 100 nm, (c) 200 nm, (d) 300 nm, (e) 400 nm, (f) 500 nm.

the stress accommodation, which results in enhanced coating properties. The critical depth due to the effect of substrate will be studied later.

### 3.2. The critical depth to coating thickness at which the contribution of the substrate is negligible

It is a well known fact that in order to measure the hardness of a coating on a substrate by indentation, the penetration depth must be less than a critical value, which is a small fraction of the thickness of the coating. The frequently used one-tenth rule suggests that if a coating has a thickness of ten times the in-

dentation depth, then the measured hardness is very close to the true hardness of the coating [18]. Therefore, a large penetration depth is not desirable as it will introduce substrate effect into coating property measurement. Indeed, the penetration depth genuinely does affect the measured hardness as shown in Fig. 9.

Therefore, the half-space method was developed in order to find out the critical penetration depth above which the substrate starts to affect the load-displacement behaviour of the coating. Figure 11 shows the load-displacement curves of the coating-substrate system and the coating half-space. It can be seen that there is no substrate effect when the penet-

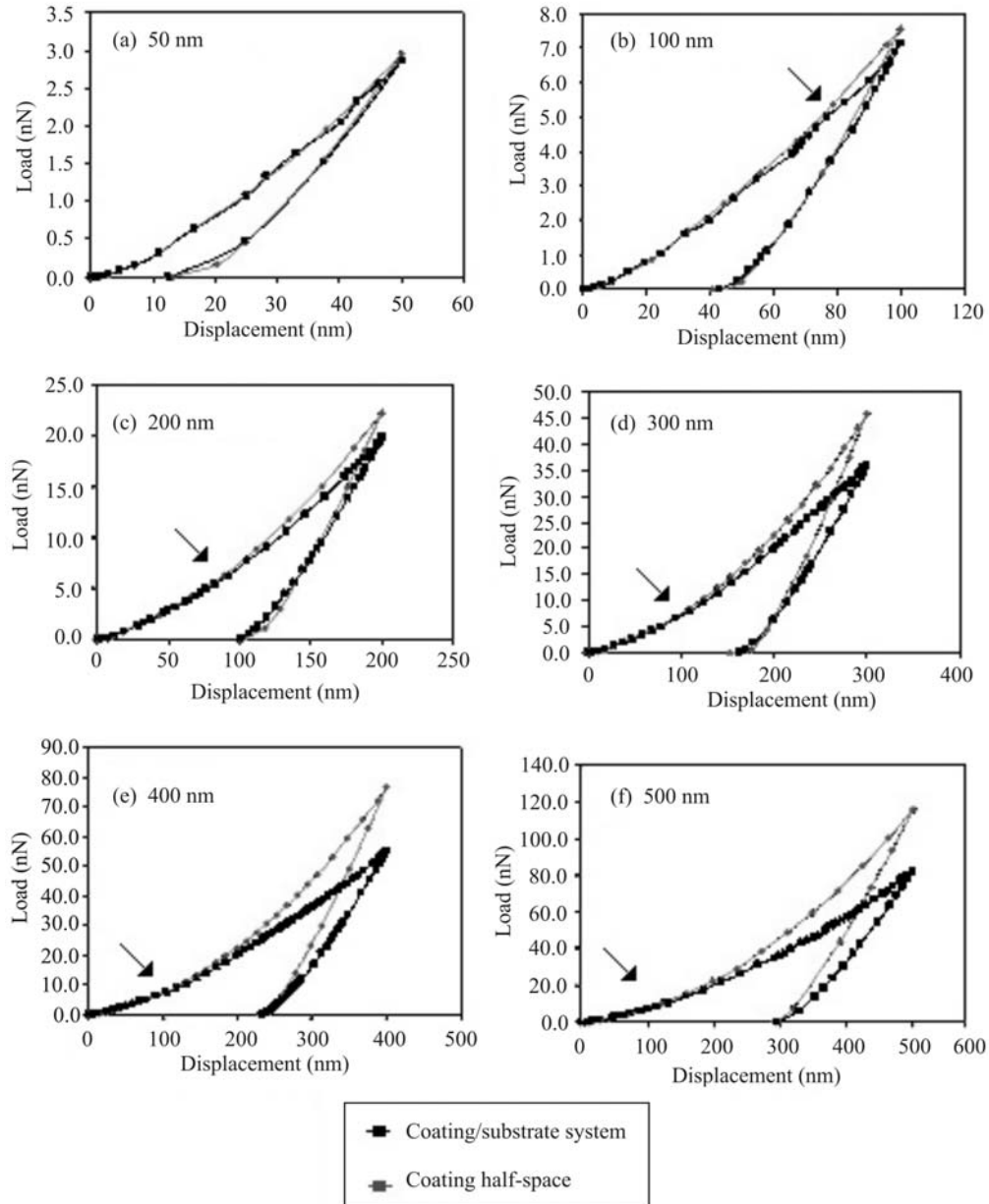


Fig. 11. Load-displacement curves of coating-substrate systems and the corresponding coating half-spaces at different indentation depths: (a) 50 nm, (b) 100 nm, (c) 200 nm, (d) 300 nm, (e) 400 nm, (f) 500 nm.

ration depth is 50 nm, since the loading-displacement curve of the coating-substrate system coincides well with that of the coating half-space. But the load-displacement curves of coating half-space start to deviate from the curves of coating-substrate system at increasing penetration depth. The penetration depth at which the deviation starts to take place (arrow) can be considered as the critical depth for the substrate to take effect. From Fig. 11, the critical depth is found to be around 92 nm, which agrees with the results shown in Fig. 9. It should be noted that the  $\text{TiB}_2$  coating thickness is  $1.4 \mu\text{m}$ . The critical depth of 92 nm corresponds to a depth-to-coating thickness ratio of 0.07,

i.e. in order to avoid substrate effect in  $\text{TiB}_2$  coating hardness measurement the indentation depth should not exceed about 7 % of the coating thickness. This is in agreement with Sun et al.'s work [19] and is in an approximation with the well known "one-tenth" rule.

## 4. Discussion

### 4.1. Sink-in effects

From Fig. 11 it can be seen that the existence of

a hard coating on a soft substrate promotes sink-in of the coating material around the indenter during nanoindentation. This observed sink-in is expected for materials with a low value of  $E/Y$  (e.g., some glasses and ceramics). The plastic zone is typically contained within the boundary of the circle of contact and the elastic deformations that accommodate the volume of the indentation are spread at a greater distance from the indenter [20]. It can also be seen that the sink-in height increases when the penetration depth increases. But the sink-in height of coating/substrate system is less than those from coating half-space when the penetration depth is above  $0.2 \mu\text{m}$  due to the substrate effect.

#### 4.2. Properties extraction

FE analysis of contact in which sink-in takes place has shown that the true contact area can be significantly smaller than that calculated from the conventional O&P method [21] (measured penetration depth and the assumed elastic unloading response). It is noted that the true properties such as true hardness and modulus can be extracted by using the true contact area obtained from the FE analysis. Since the true contact area calculated from FE analysis is smaller than the measured one, the hardness calculated from the true contact area should be larger than the value obtained from experiment. This is the reason why the hardness values calculated by FE calculation (true hardness) are slightly higher than the experimental ones (Fig. 9) at various penetration depths.

On the other hand, if pile-up occurs, the true contact area can be significantly greater than that calculated using the conventional method, resulting in the lower hardness values from the true hardness calculation. In addition, the effect of sink-in and pile-up on the contact area can cause the errors in contact area of up to 60 % [22]. Thus, sink-in and pile-up can have detrimental effect on the determination of the area function of the indenter if the specimen used for the examination of the area function behaves differently [20]. With the use of the FE technique, the determination of the true mechanical properties can be obtained.

#### 4.3. Plastic zone deformation

From Fig. 10 it can be seen that substrate effect starts when the plastic zone in the coating reaches the interface and thus it is actually initiated before substrate deformation. The vertical constraint of the plastic zone at the interface is accommodated by the lateral development of the zone, which results in further material sink-in around the indenter.

#### 4.4. Critical depth

From the present model, the critical indentation depth-to-coating thickness ratio at which the contribution of the substrate is negligible could be found. This is beneficial to extract the intrinsic mechanical properties of the coating without the effect from the substrate. From Fig. 11, the critical depth is found to be around 92 nm. It should be noted that the  $\text{TiB}_2$  coating thickness in the model is  $1.4 \mu\text{m}$ . The critical depth of 92 nm corresponds to a depth-to-coating thickness ratio of 0.07, i.e. in order to avoid substrate effect in  $\text{TiB}_2$  coating hardness measurement, the indentation depth should not exceed about 7 % of the coating thickness. This is in agreement with Sun et al.'s work [19]. In addition, it should be pointed out that the frequently used one-tenth "rule of thumb" does not apply for  $\text{TiB}_2$  coating property measurement (ultra-hard coating). For the wide range of coatings investigated, the coating hardness can be safely measured if the indentation depth is less than 7 % of the coating thickness.

### 5. Conclusions

Since finite element models have been developed to simulate the nanoindentation response of the coating systems, the following conclusions can be drawn regarding the FE analysis:

1. The models have the ability to simulate the loading and unloading stages, the plastic deformation behaviour of the coating and the substrate, extract the mechanical properties of the coating, and simulate the complicated coating behaviour during indentation such as sink-in effect.
2. The developed models have been successfully used together with the nanoindentation experiments to extract intrinsic yield strength value for selected  $\text{TiB}_2$ -based coatings.
3. In order to avoid substrate effect in  $\text{TiB}_2$  coating hardness measurement, the indentation depth should not exceed about 7 % of the coating thickness.

### Acknowledgements

Authors would like to thank School of Materials Science and Engineering, Nanyang Technological University, Singapore for technical assistance.

### References

- [1] BHATTACHARYA, A. K.—NIX, W. D.: International Journal of Solids and Structures, 24, 1998, p. 1287.
- [2] BHATTACHARYA, A. K.—NIX, W. D.: International Journal of Solids and Structures, 27, 1991, p. 1047.

- [3] SUN, Y.—BLOYCE, A.—BELL, T.: *Thin Solid Films*, 271, 1955, p. 122.
- [4] CHOLLACOOPE, N.—DAO, M.—SURESH, S.: *Acta Materialia*, 51, 2003, p. 3713.
- [5] LICHINCHI, M.—LENARDI, C.—HAUPT, J.—VITALI, R.: *Thin Solid Films*, 333, 1998, p. 278.
- [6] WANG, H. F.—BANGERT, H.: *Materials Science and Engineering A*, 163, 1993, p. 43.
- [7] KNAPP, J. A.—FOLLSTAEDT, D. M.: *Surface Coatings and Technology*, 103–104, 1998, p. 268.
- [8] MULIANA, A.—STEWART, R.—HAJ-ALI, R. M.—SAXENA, A.: *Metallurgical and Materials Transactions A*, 33A, 2002, p. 1939.
- [9] KENNEDY, F. E.—LING, F. F.: *ASME J. Eng. Mater. Technol.*, 96, 1974, p. 97.
- [10] KOMVOPOULOS, K.: *ASME Journal of Tribology*, 111, 1989, p. 430.
- [11] TIAN, H.—SAKA, N.: *ASME Journal of Tribology*, 148, 1991, p. 47.
- [12] MONTMITONNET, P.—EDLINGER, M. L.—FELDER, E.: *ASME Journal of Tribology*, 115, 1993, p. 15.
- [13] DJABELLA, H.—ARNELL, R. D.: *Thin Solid Films*, 235, 1993, p. 156.
- [14] ABAQUS User Manual (version 6.3). Pawtucket, Hibbitt, Karlsson & Sorensen, Inc. 1998.
- [15] PANICH, N.—SUN, Y.: *Thin Solid Films*, 500, 2006, p. 190.
- [16] BALSHAKOV, A.—PHARR, G. M.: *Journal of Materials Research*, 13, 1998, p. 1049.
- [17] LARSSON, M.—BROMARK, M.—HEDENQVIST, P.—HOGMARK, S.: *Surface Coatings and Technology*, 76/77, 1995, p. 202.
- [18] PEGGS, G. N.—LEIGH, I. C.: Recommended procedure for micro-indentation Vickers hardness test. Report MOM 62. London, UK National Physical Laboratory 1983.
- [19] SUN, Y.—BELL, T.—ZHENG, S.: *Thin Solid Films*, 258, 1995, p. 198.
- [20] FISCHER-CRIPPS, A. C.: *Nanoindentation*. New York, Springer-Verlag 2002.
- [21] OLIVER, W. C.—PHARR, G. M.: *Journal of Materials Research*, 7, 1992, p. 1564.
- [22] BALSHAKOV, A.—PHARR, G. M.: *Journal of Materials Research*, 13, 1998, p. 1049.